Supplementary File

Visible light photoreforming of Greenhouse gases by nano Cu-Al LDH intercalated with urea-derived anions

Ayat A.-E. Sakr [a,*], Dalia R. Abd El-Hafiz [b], Osama Elgabry [a], Eman S. Abdullah [a], Mohamed A. Ebiad [a], Tamer Zaki [b]

[a] *Analysis & Evaluation Division, Egyptian Petroleum Research Institute, Nasr city, P.B. 11727, Cairo, Egypt*

[b] *Catalysis Department, Petroleum Refining Division, Egyptian Petroleum Research Institute, Nasr city, P.B. 11727, Cairo, Egypt.*

** Corresponding author*

E-mail: ayatsakr@yahoo.com; ayatsakr78@gmail.com; ayatsakr@epri.sci.eg

ORCID ID: 0000-0003-1987-0869

Table S1: previously reported synthesizes Cu-Al LDH homogenously precipitated by urea hydrolysis.

Material	*Source*	*Reactor*	*Temperature*	*Pressure*	*Heating source*	*Application*	*References*
Cu-Al LDH	**Cu/Al-nitrates**	**Open glass reactor**	**~95℃ for 1.5 h**	**Atmospheric pressure**	**MW**	**Photocatalytic greenhouse gases (CO_2, CH_4, and H_2O) reforming**	**This work**
Cu-Al LDH/ Zn-BTC	Cu/Al-nitrates	Teflon-lined stainless-steel autoclave	130 ℃ for 8 h	Under hydrothermal conditions	thermal	CO_2 hydrogenation to methanol	1
Cu-Al LDH	Cu/Al-nitrates, dimethyl sulfoxide (DMSO)	Teflon-lined stainless-steel autoclave	110 ℃ for 12 h	Under hydrothermal conditions	thermal	methyl orange degradation	2
Cu-Al LDH/PVDF composite	Cu/Al-nitrates	Teflon-lined stainless-steel autoclave	100 ℃ for 6 h	Under hydrothermal conditions	thermal	Dye removal from water	3
Modified Cu-Al LDH	Cu/Al-nitrates, DMSO as the solvent	Teflon-lined stainless-steel autoclave	110 ℃ for 12 h.	Under hydrothermal conditions	thermal	nano-scale drug delivery system	4
Cu–Al LDH/g-C3N4 nanocomposites	Cu/Al-nitrates	Teflon-lined stainless-steel autoclave	130 ℃for 4 h	Under hydrothermal conditions	thermal	supercapacitors	5
polymers-decorated Cu-Al LDH	Cu/Al-nitrates, DMSO as the solvent	Teflon-lined stainless-steel autoclave	110 ℃ for 12 h.	Under hydrothermal conditions	thermal	Photothermal therapy	6
diatomite/Cu-Al LDH hybrid composite	Cu/Al-nitrates	Teflon-lined stainless-steel autoclave	110 ℃ for 18 h	Under hydrothermal conditions	thermal	polyethylene degradation	7
Cu-Al LDH microsphere	Cu/Al-sulphates	--	100 ℃ for 24 h under stirring	--	Thermal	Non-enzymatic glucose sensor	8
Cu-Al LDH intercalated with molecular metallo-porphyrins	Cu/Al-nitrates	Teflon-lined stainless-steel autoclave	130 ℃for 8 h	Under hydrothermal conditions	thermal	CO2 hydrogenation	9
Metal oxides derived Cu-Al LDH	Cu/Al-nitrates	Teflon-lined stainless-steel autoclave	110 ℃ for 12 h	Under hydrothermal conditions	thermal	Electrocatalytic nitrate conversion	10
Hierarchical Cu-Al LDH/carbon fiber composites	Cu/Al-nitrates	Teflon-lined stainless-steel autoclave	110 ℃ for 12 h	Under hydrothermal conditions	thermal	Degradation of ammonia nitrogen from wastewater.	11

Sec. S1: Experimental

In more detail, regarding the quality and purity of the raw materials, for the synthesis of C4 material (as an example), in 500 mL of deionized water, a mixture of 9.15 g of copper nitrate, 4.78 g of aluminium nitrate, and 21.12 g of urea was prepared. The mixture is then subjected to microwave irradiation (270 watts) under continuous stirring for 90 minutes. A precipitate was formed and then treated as mentioned in Section 2.1.

Sec. S2

pH monitoring of Cu-Al LDH synthesis reaction

Several pH changes are observed during the synthesis reaction as a result of urea hydrolysis and metal precursor precipitation (Figures (S1-S3) and Tables (S2-S4)). Microwave irradiation is a green source of energy that produces fast and uniform heating. Using MW in this type of synthesis reaction provides less energy consumption and reaction time and results in the formation of nearly homogeneous particle morphology [12,13]. In addition, MW irradiation breaks down the formed urea-metal complex, producing metal hydroxide precipitates [14]. MW enhances the decomposition of urea, which consequently increases the supersaturation of the solution, which leads to the spontaneous increase of the solution pH. The extent of supersaturation is affected mainly by the urea concentration. It is responsible for the formation of nuclei and their growth into final particles [15]. Figures S1–S3 represent the pH changes as a function of time.

Regarding the pH changes during the LDH synthesis reaction, different regions are observed:

1- At the initial reaction stage, the concentrations of the positive species (metal cations and H^+ from water dissociation) are rather high. Region I is characterized by a decrease in the pH value. This may be due to the high consumption rate of the released OH anions from urea hydrolysis by the solution-positive species [16,17].
2- The sharp increase in pH (II and IV) regions may be due to the release of excess OH ions in the solution due to the urea hydrolysis process [17,18].
3- The plateau regions (III and IV) could be due to the successive metal hydroxide formations giving rise to the formation of positively charged layers [15,18,19]. Furthermore, the different plateau regions may indicate the intercalation of different anionic groups within the layered structures [20].

4- A colloidal suspension is observed after the first plateau at pH > 4 due to the LDH primary particles [18]. With further increases in pH, particles aggregate to form a precipitate [17].

Figure S1 and Table S1 represent the effect of MW power on Cu-Al LDH materials prepared at the same periods, metals, and urea concentrations. As the MW power increases, the reaction rate represented during the pH change regions is accelerated, and the final pH values are increased.

The effect of urea concentration on the pH changes of the Cu-Al LDH synthesis (Figure S2 and Table S3) indicates that the precipitation reaction rate increases as the urea concentration increases [19]. For low urea concentrations (C6 and C7), the final pH values were low, and the precipitates obtained were very poor. Moreover, the final pH of the C9 (Figure S4) sample was 3.39, and the resulting ppt was too low under the synthesis conditions. This sample will not be considered for further investigation in this study.

Regarding the effect of the M^{II}/M^{III} ratio (Figure S3 and Table S3), the final pH increases as the metal ratio increases. This may be due to the high charge density of the M^{III} ions, which consume a higher amount of hydroxide ions. Thus, for samples prepared at the same time and with the same urea concentration, a lower final pH is observed for high M^{III} concentrations.

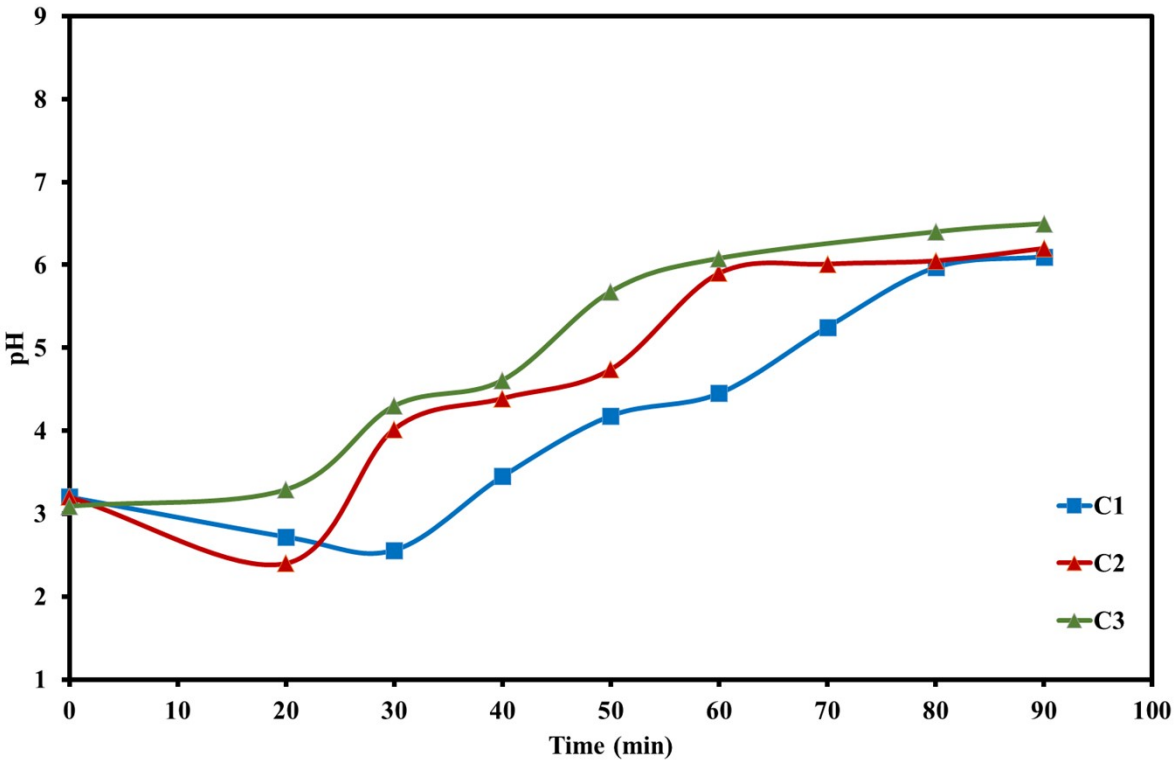

Fig. S1: Effect of MW power on pH changes during Cu-Al LDH synthesis reaction.

Table S2: Effect of MW power on the pH change during homogenous precipitation of the Cu-Al LDH materials prepared at the same conditions.

Material	Region (I) (gradual decrease)	Region (II) (sharp increase)	Region (III) (Plateau)	Region (IV) (sharp increase)	Region (V) (Plateau)	Final pH
C1	3.2 – 2.56	2.56 – 4.18	4.18 – 4.45	4.45-6.05	6.05-6.1	6.1
C2	3.45 – 2.4	2.4 – 4.39	4.39-4.74	• 4.74-5.9 • 4.61-5.68	5.9-6.2	6.2
C3	3.09 – 3.29	2.66 – 4.3	4.3-4.61	5.68-6.48 (slow increase)	6.48-6.5	6.5

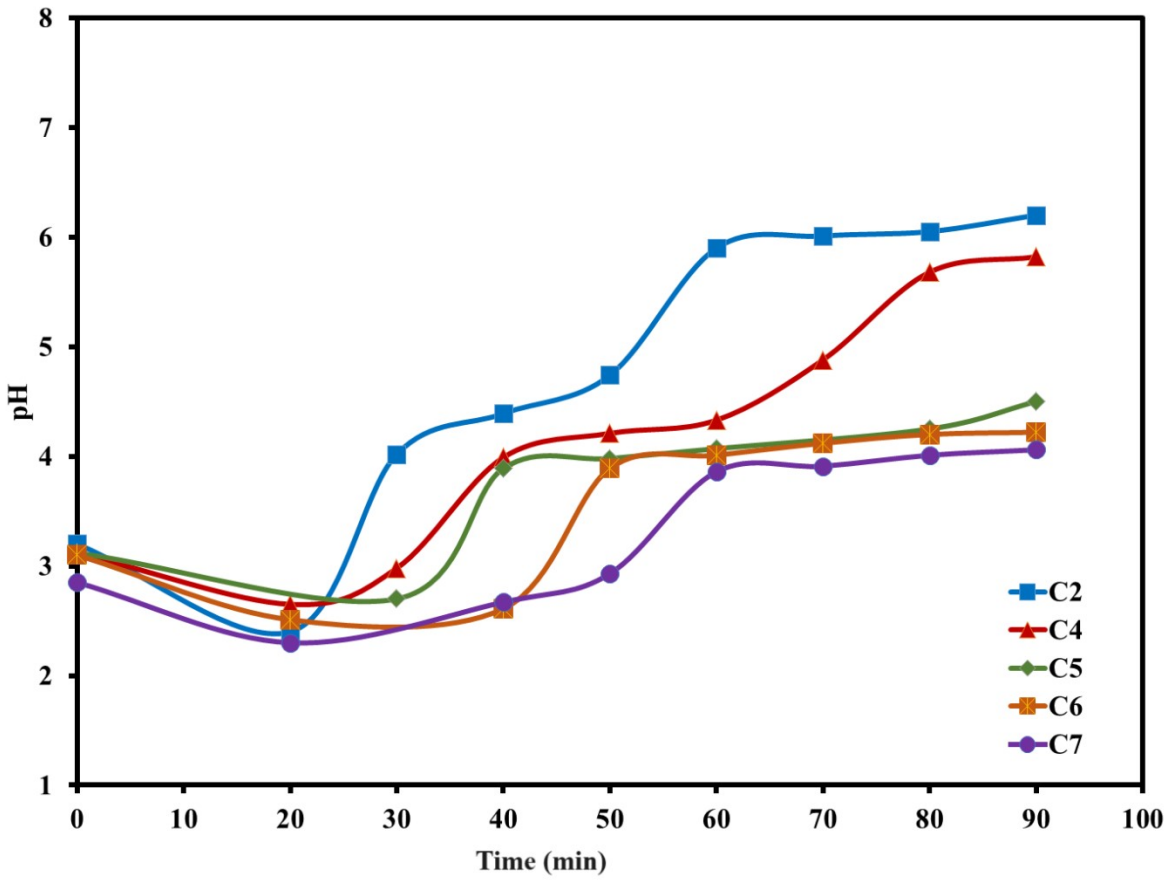

Fig. S2: Effect of urea concentration on pH changes during Cu-Al LDH synthesis reaction.

Table S3: Effect of urea concentration on the pH change during homogenous precipitation of the Cu-Al LDH materials prepared at the same conditions.

Material	Region (I) (gradual decrease)	Region (I-1) (plateau)	Region (II) (sharp increase)	Region (III) (Plateau)	Region (IV) (sharp increase)	Region (V) (Plateau)	Final pH
C2	3.45 – 2.4	--	2.4 – 4.39	4.39-4.74	4.74-5.9	5.9-6.2	6.2
C4	3.12-2.65	--	2.65-3.99	3.99-4.33	4.33-6.68	5.68-5.82	5.82
C5	3.12-2.7	--	2.7-3.89	3.89-4.25	4.25-4.5	--	4.5
C6	3.10-2.51	2.51-2.61	2.61-3.89	3.89-4.22	--	--	4.22
C7	2.85-2.3	2.3-2.93	2.93-3.86	3.86-4.06	--	--	4.06

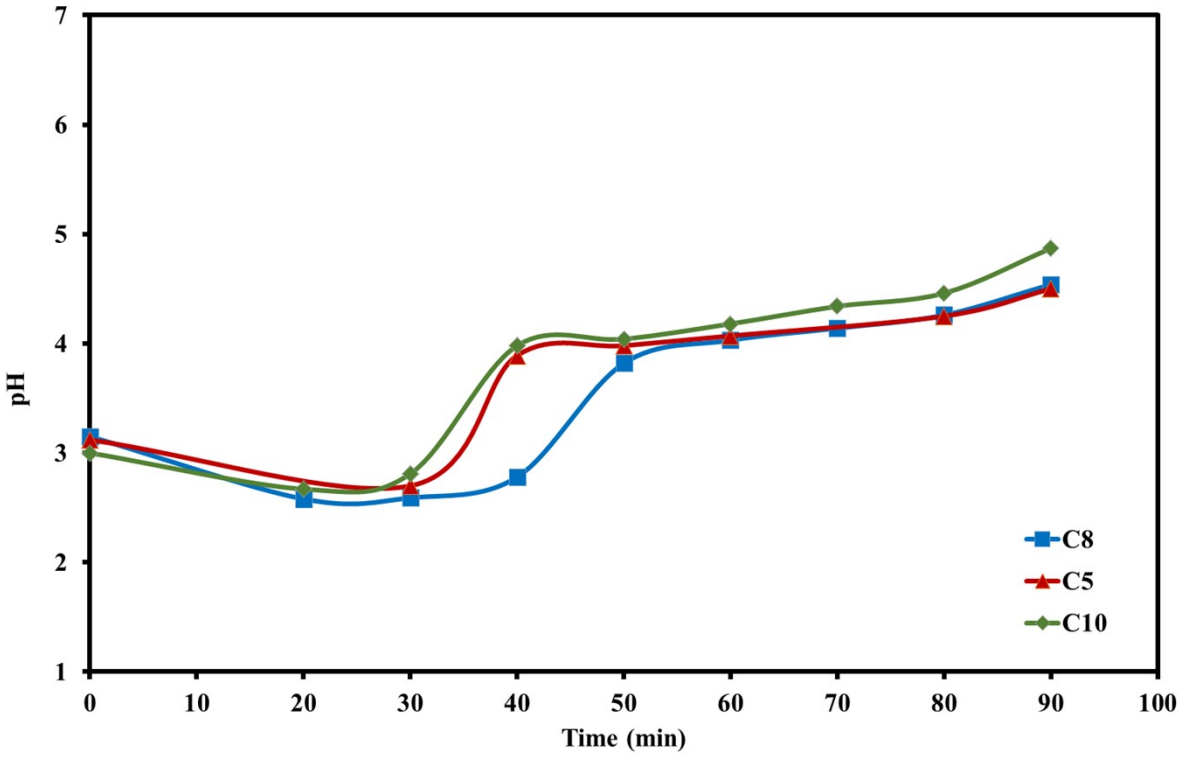

Fig. S3: Effect of MII/MIII ratio on the pH change during homogenous precipitation of the Cu-Al LDH materials prepared at the same conditions.

Table S4: Effect of MII/MIII on the pH change during homogenous precipitation of the Cu-Al LDH materials prepared at the same conditions.

Material	Region (I) (gradual decrease)	Region (I-1) (plateau)	Region (II) (sharp increase)	Region (III) (Plateau)	Region (IV) (sharp increase)	Region (V) (Plateau)	Final pH
C8	3.15-2.58	2.58-2.78	2.78-3.82	3.82-4.26	4.26-4.54	--	4.54
C5	3.12-2.7	--	2.7-3.89	3.89-4.25	4.25-4.5	--	4.5
C10	3.0-2.81	--	2.81-3.98	3.98-4.46	4.46-4.8	--	4.87

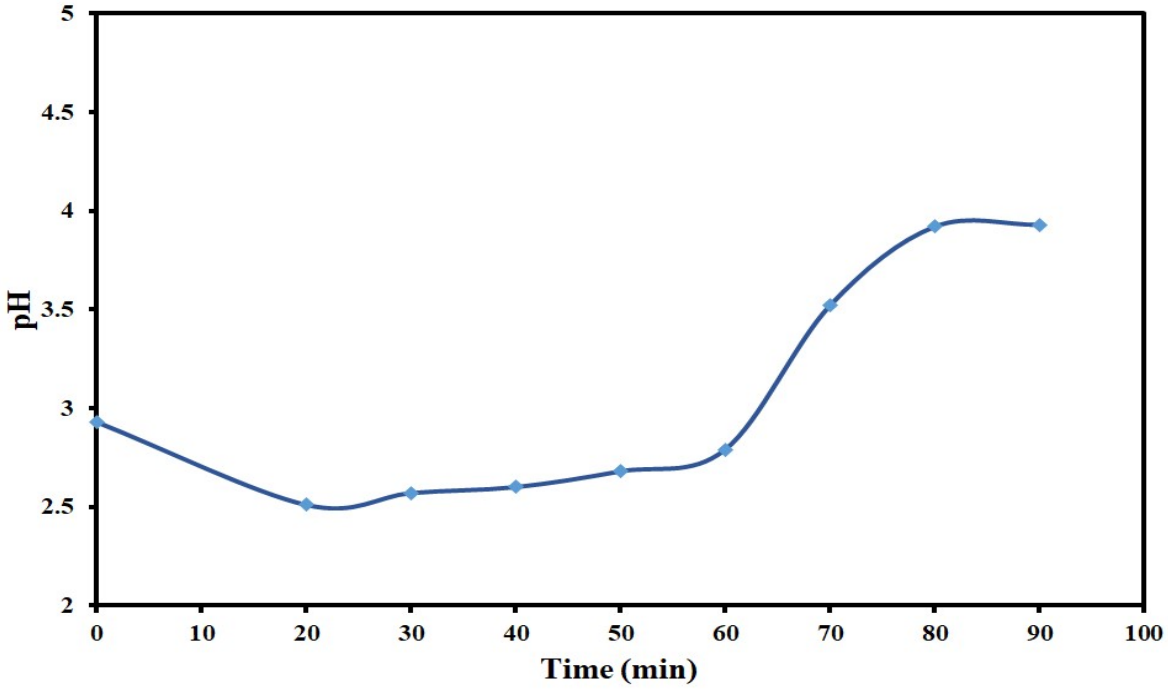

Fig. S4: pH Changes during the C9 synthesis reaction.

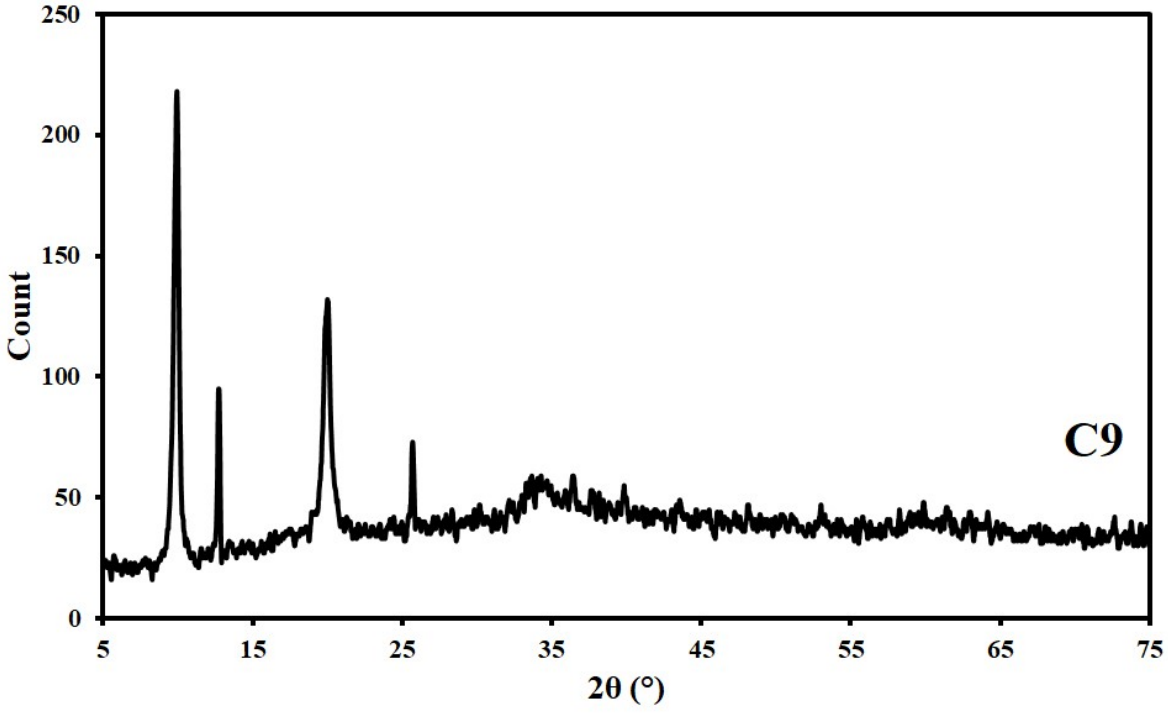

Fig. S5: C9 sample XRD pattern.

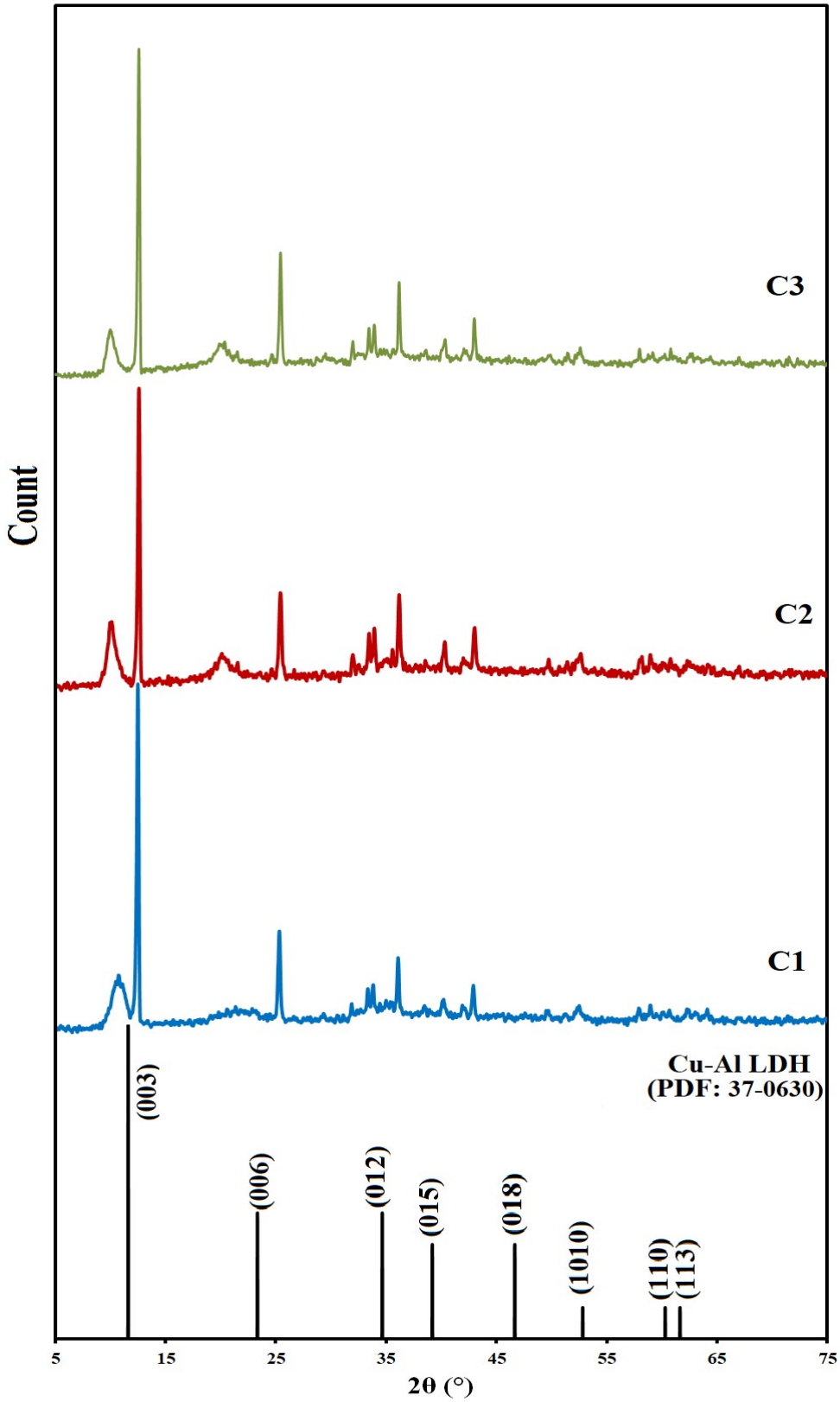

Fig. S6: XRD patterns of materials prepared at different MW power.

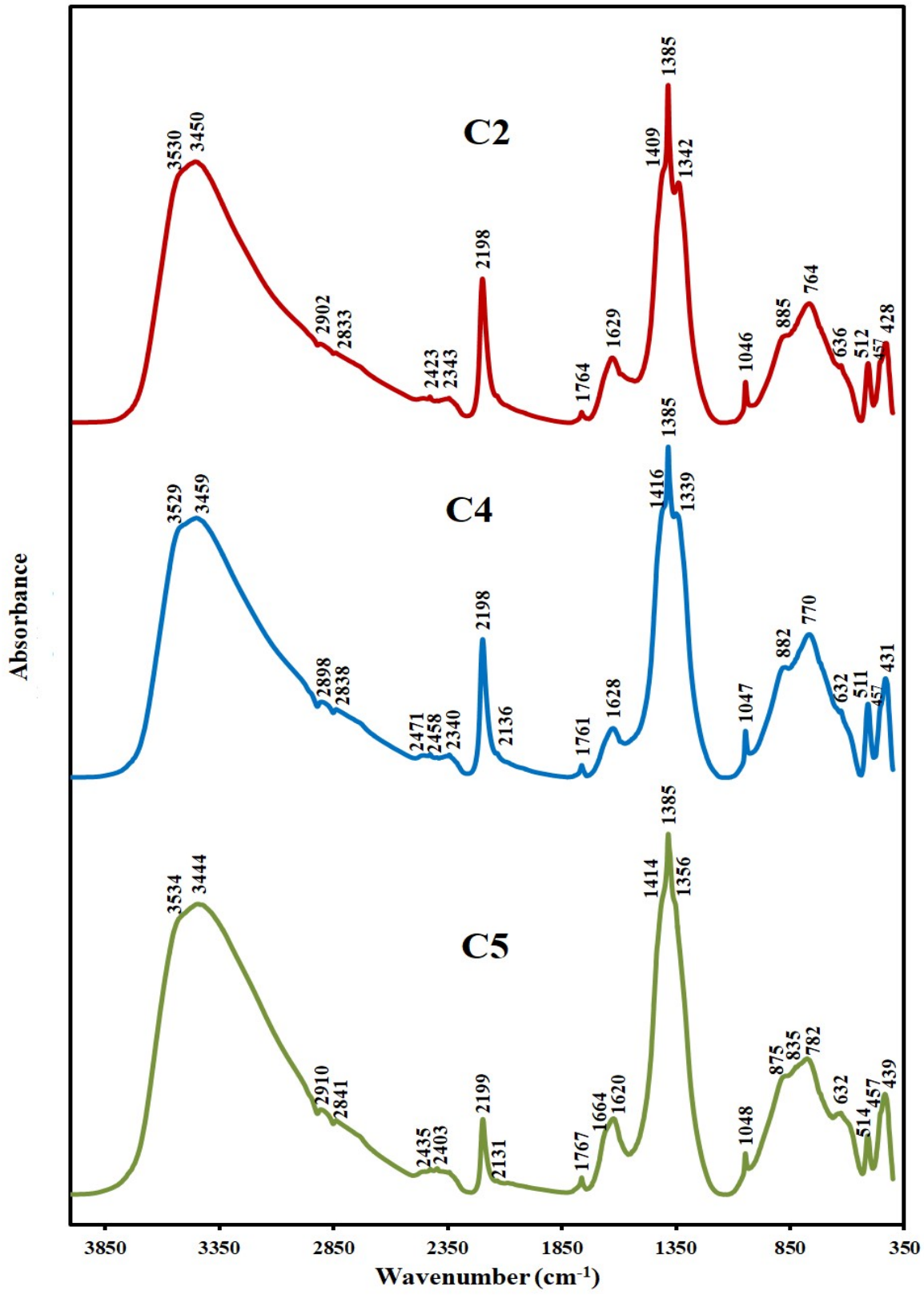

Fig. S7: Effect of varying urea concentration on the FTIR spectra of the prepared samples.

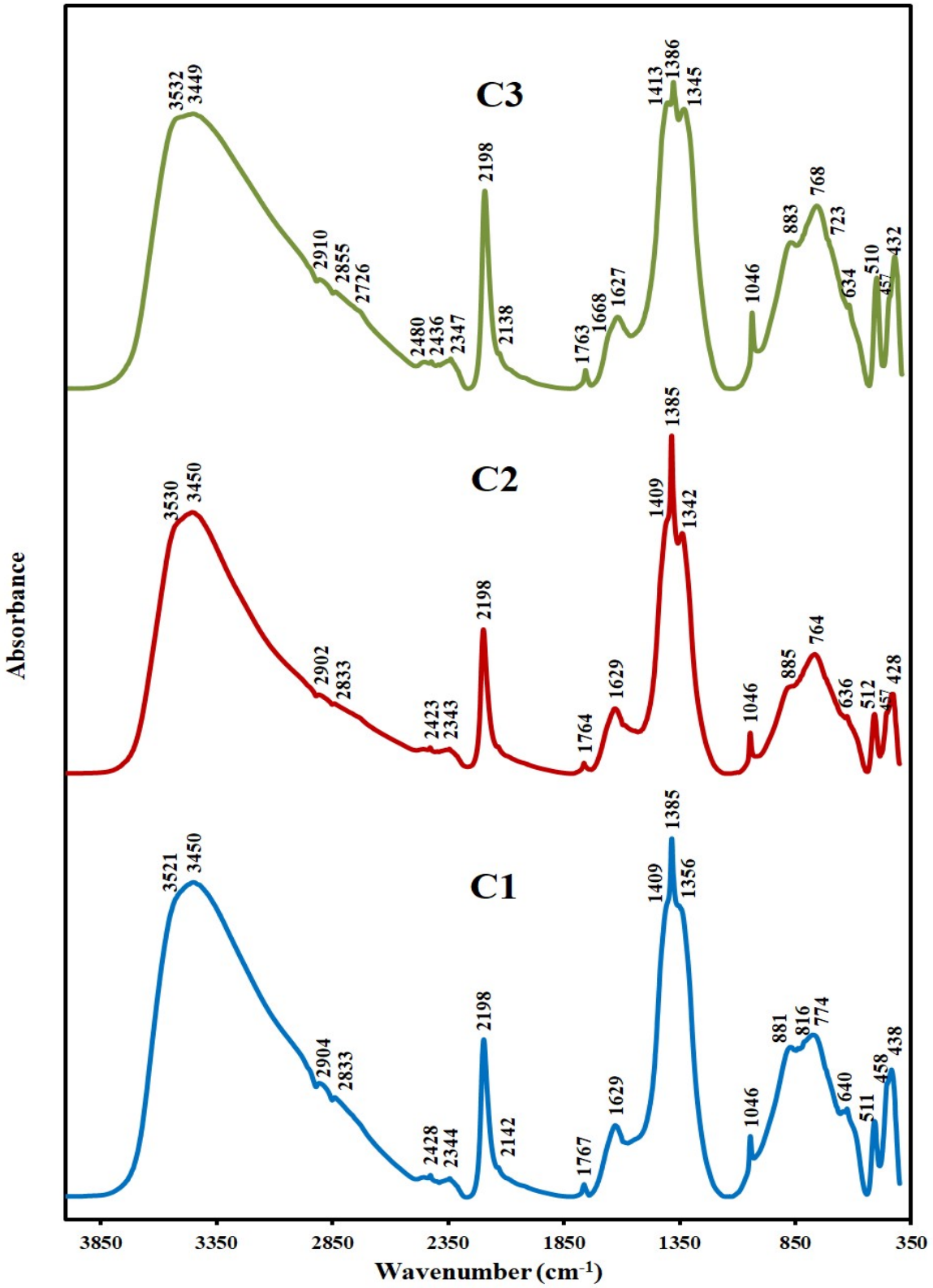

Fig. S8: Effect of varying MW power on the FTIR spectra of the prepared samples.

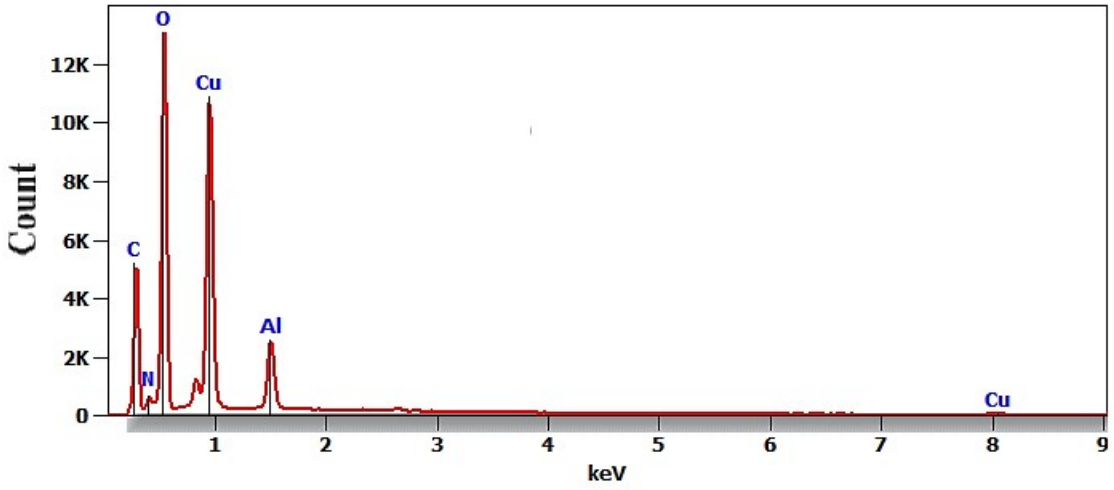

Fig. S9 : EDX analysis for C4 LDH sample.

Table S5 : EDX results for C4 LDH sample as elments %

Element	*Atom %*
C	19.37
N	4.32
O	49.05
Al	6.15
Cu	21.11

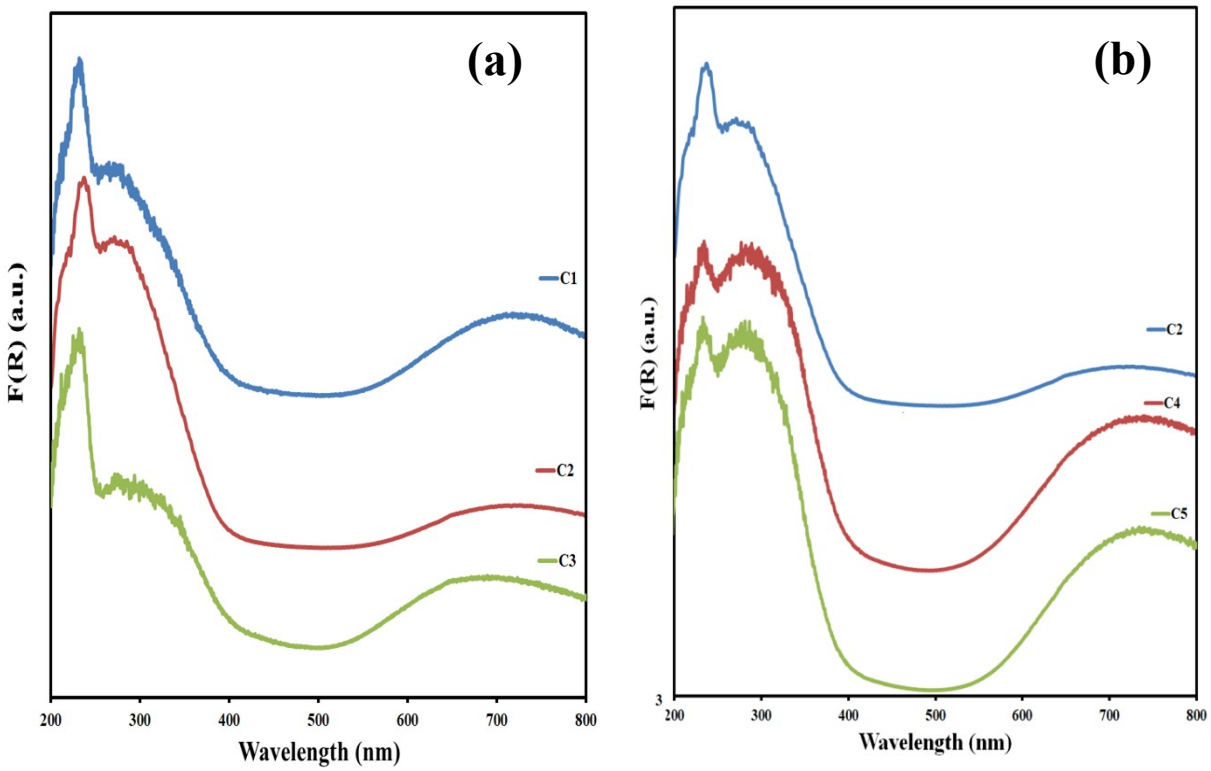

Fig. S10: DR UV-Vis spectra for samples prepared at different (a) MW power and (b) urea concentration, respectively.

Sec.3

DR UV-Vis calculation

The energy band gap (*Eg*) can be estimated using the Tauc method (which is applied to amorphous and crystalline nanomaterials) as follows:

$$(\propto h\nu)^{1/n} = A(h\nu - E_g) \quad (2)$$

where A is the proportionality constant and $h\nu$ is the photon energy (eV). The value of (*n*) determines the type of semiconductor optical transition, where n=1/2 and 2 for direct or indirect transition, respectively [21].

$$E_g = h\nu = h\frac{C}{\lambda} = \frac{1240}{\lambda}(nm) \quad (3)$$

where *h* is the Plank constant (4.136 1015 eV S^{-1}), ν is the light frequency *C* is the speed of light, and λ is the light wavelength (nm). E_g (eV) is calculated from the extrapolation of the linear proportion of the plot of $(\propto h\nu)^{1/n}$ vs. $h\nu$ [21–23].

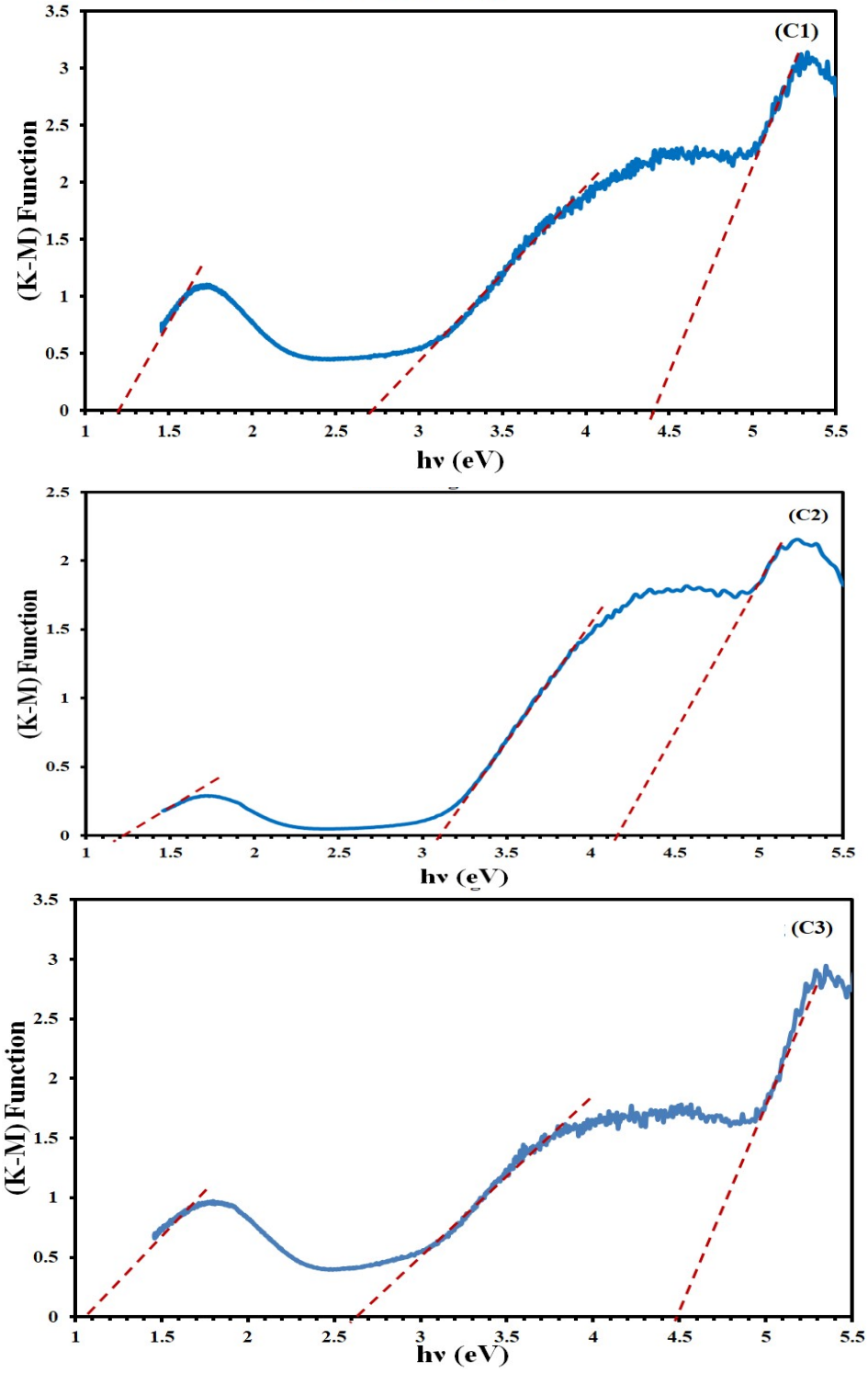

Fig. S11: Effect of MW power on the calculated energy band gaps for the Cu-Al LDH materials.

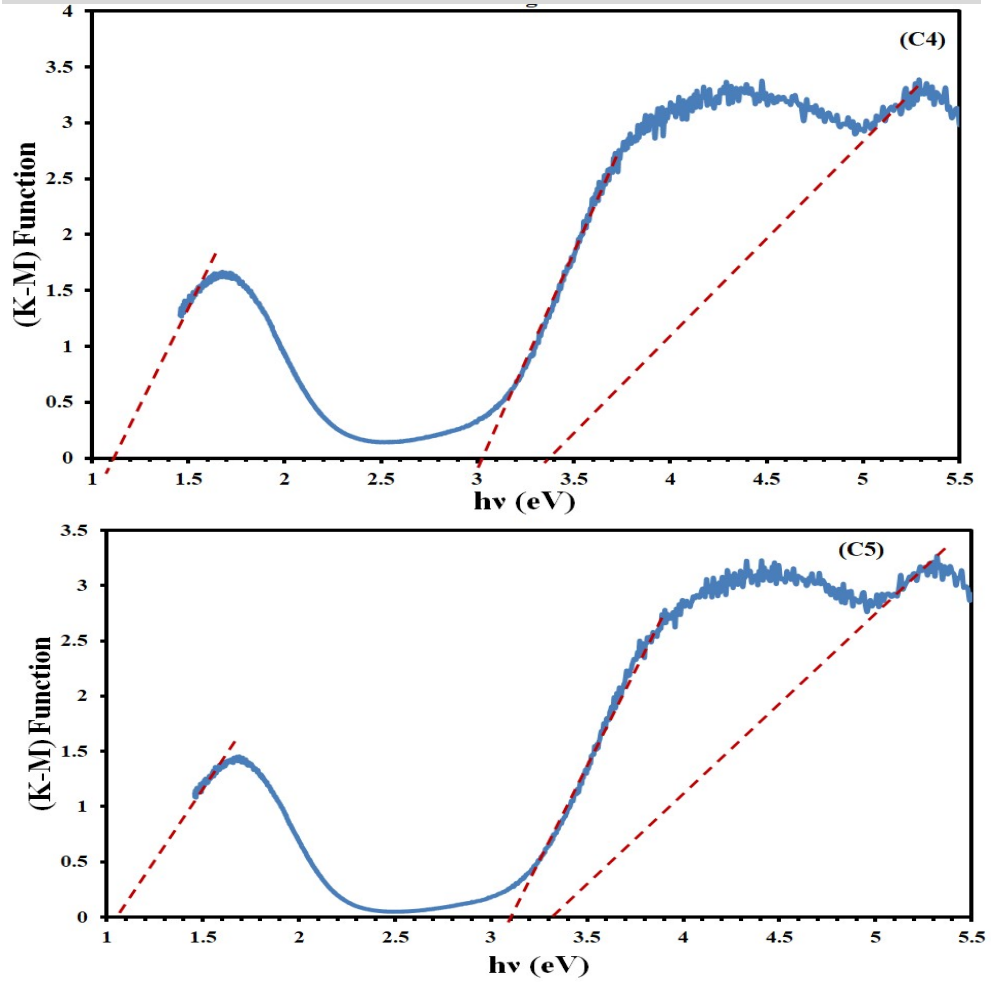

Fig. S12: Effect of varying urea concentration on the calculated energy band gaps for the Cu-Al LDH materials.

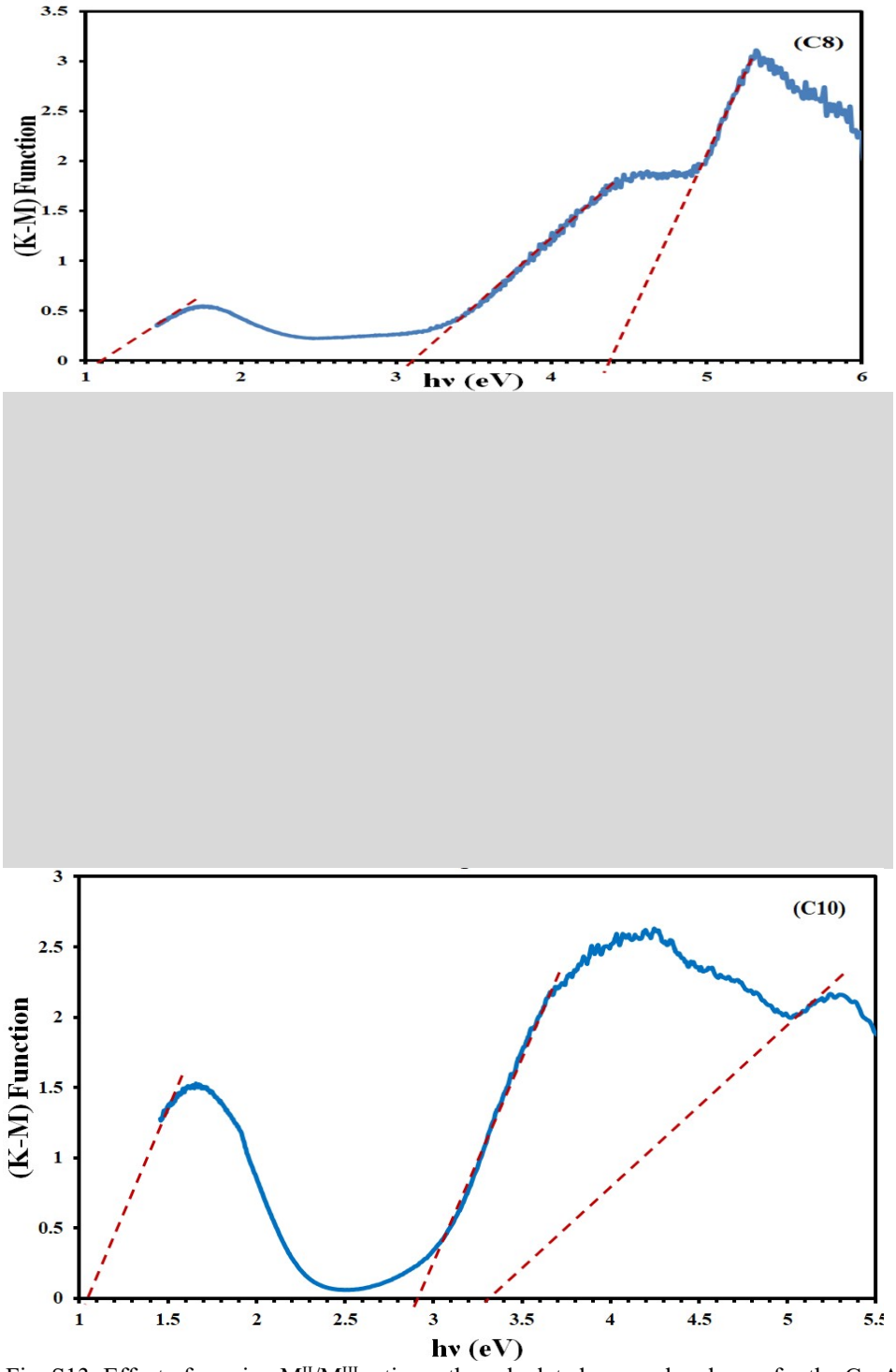

Fig. S13: Effect of varying M^{II}/M^{III} ratio on the calculated energy band gaps for the Cu-Al LDH materials.

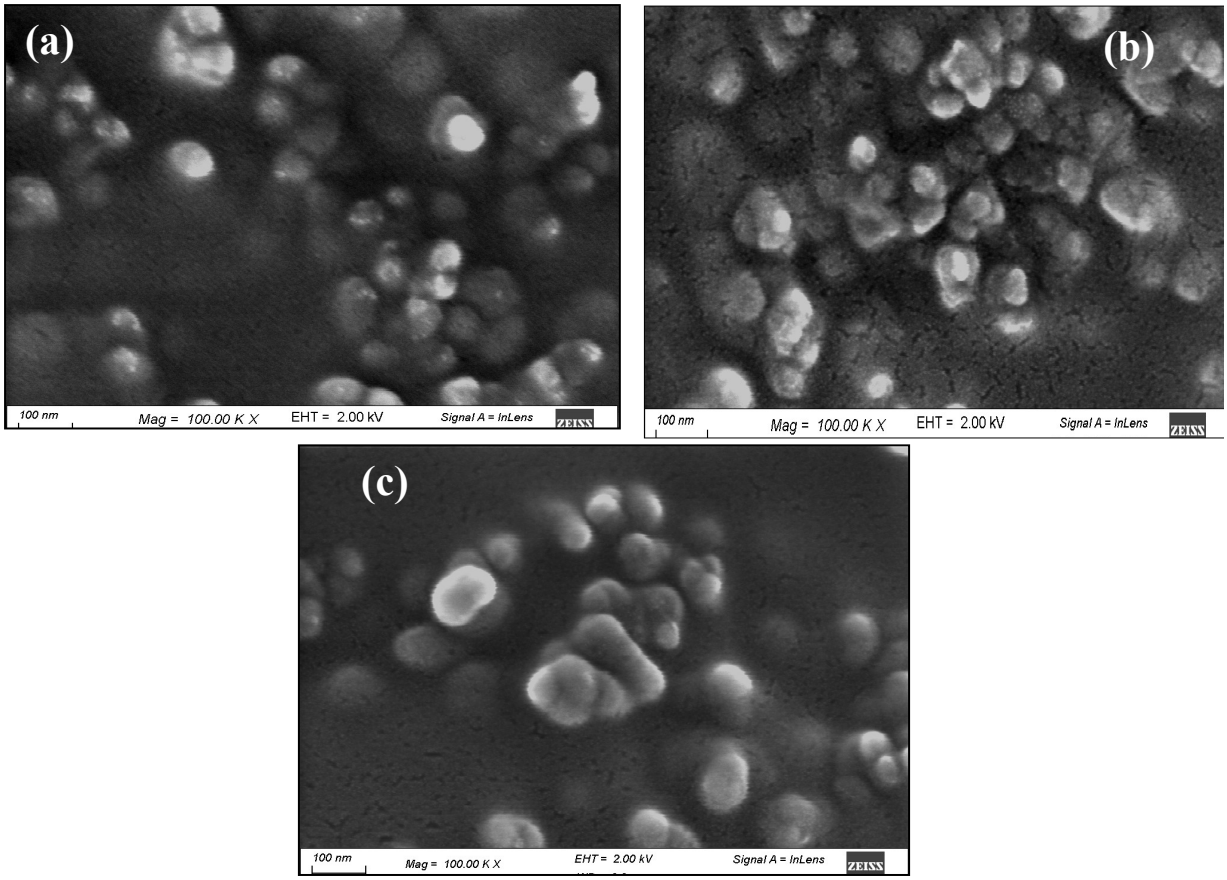

Fig. S14: FE-SEM images for a) C2, b) C4, and c) C5 Cu-Al LDH materials that are prepared at different urea concentrations.

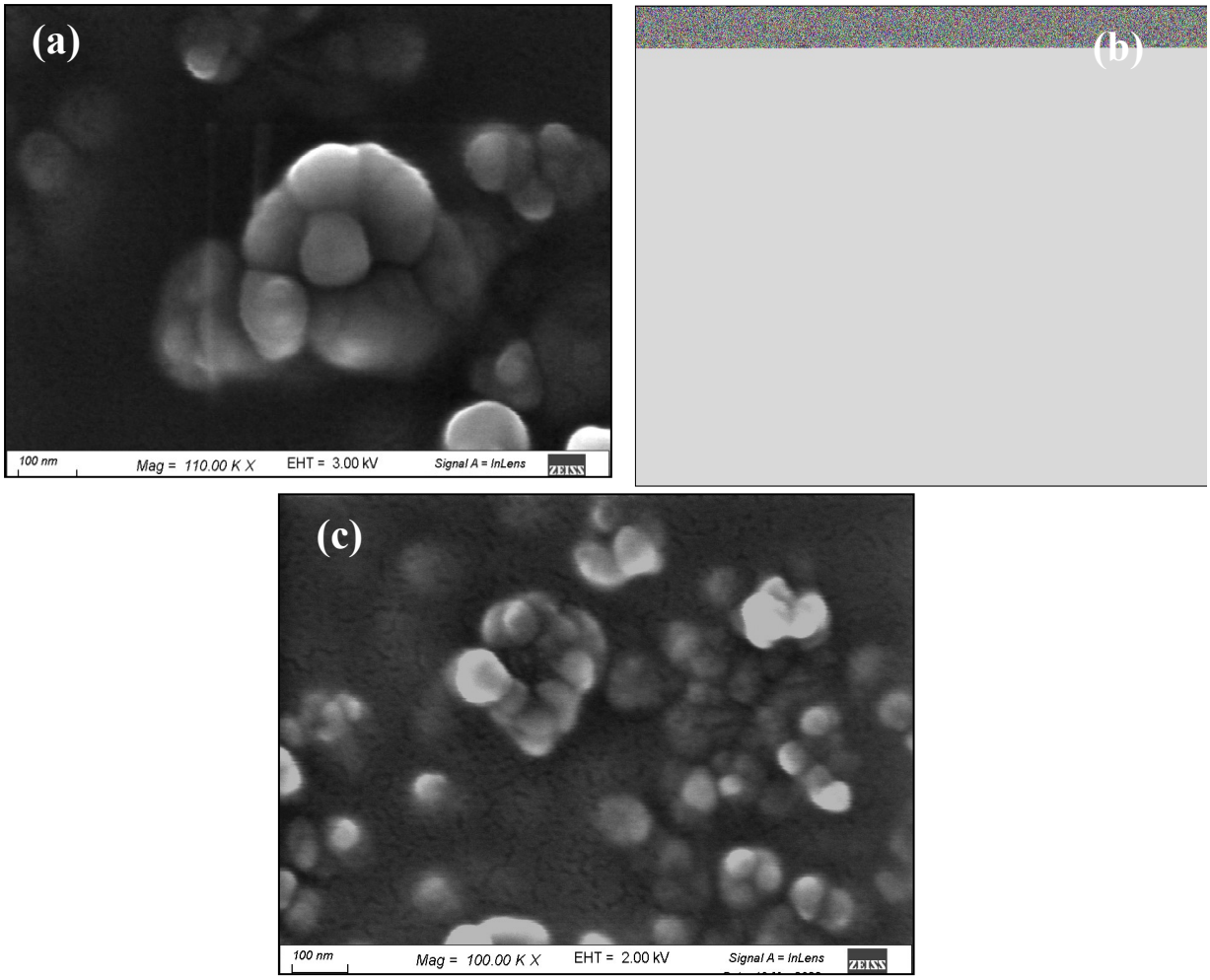

Fig. S15: FE-SEM images for a) C1, b) C2, and c) C3 Cu-Al LDH materials that are prepared at different MW power.

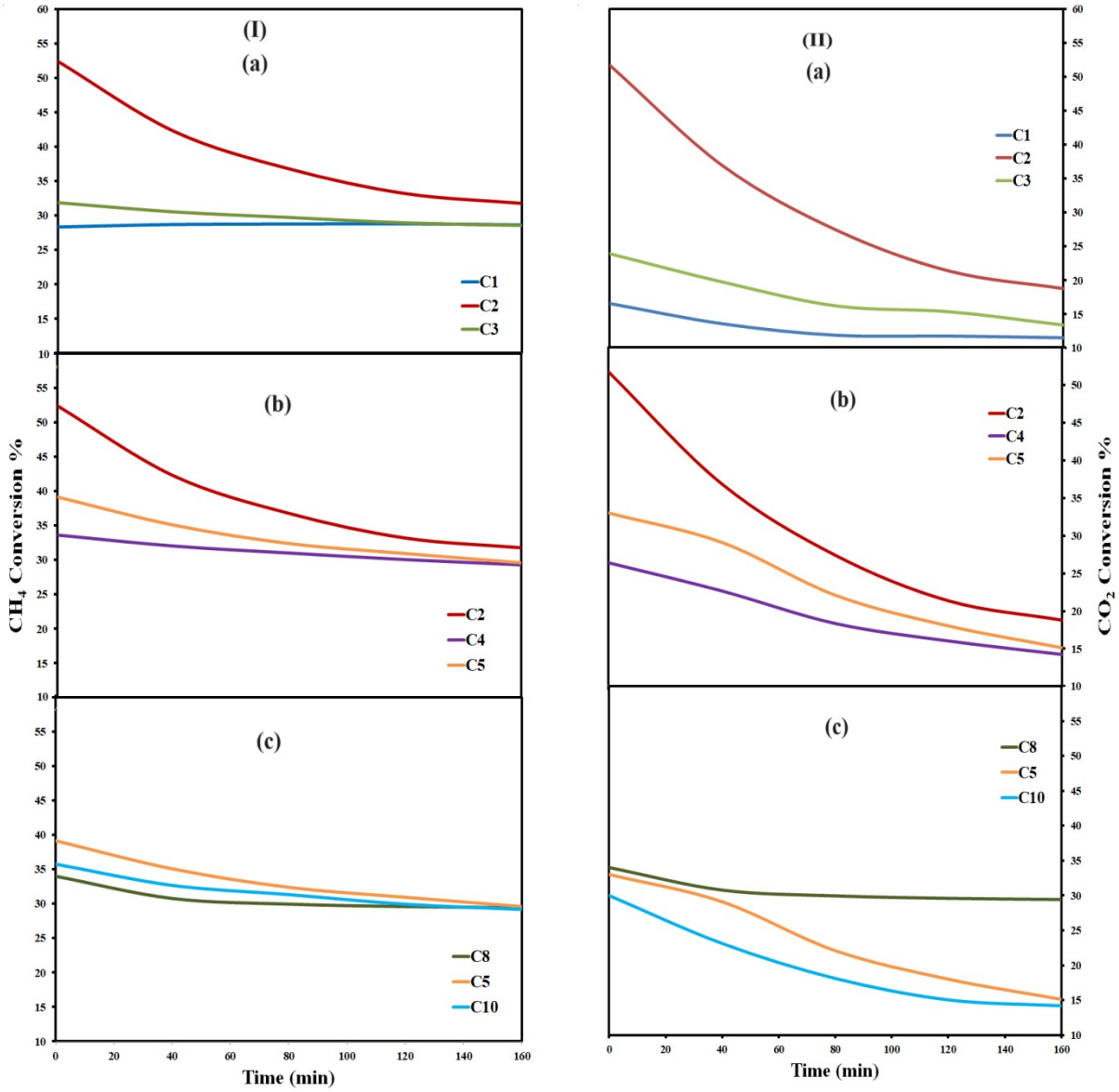

Fig. S16: Variation of (I) CH_4 and (II) CO_2 conversion % of catalysts prepared at different (a) MW power, (b) urea presentage, and (c) M^{II}/M^{III} ratios.

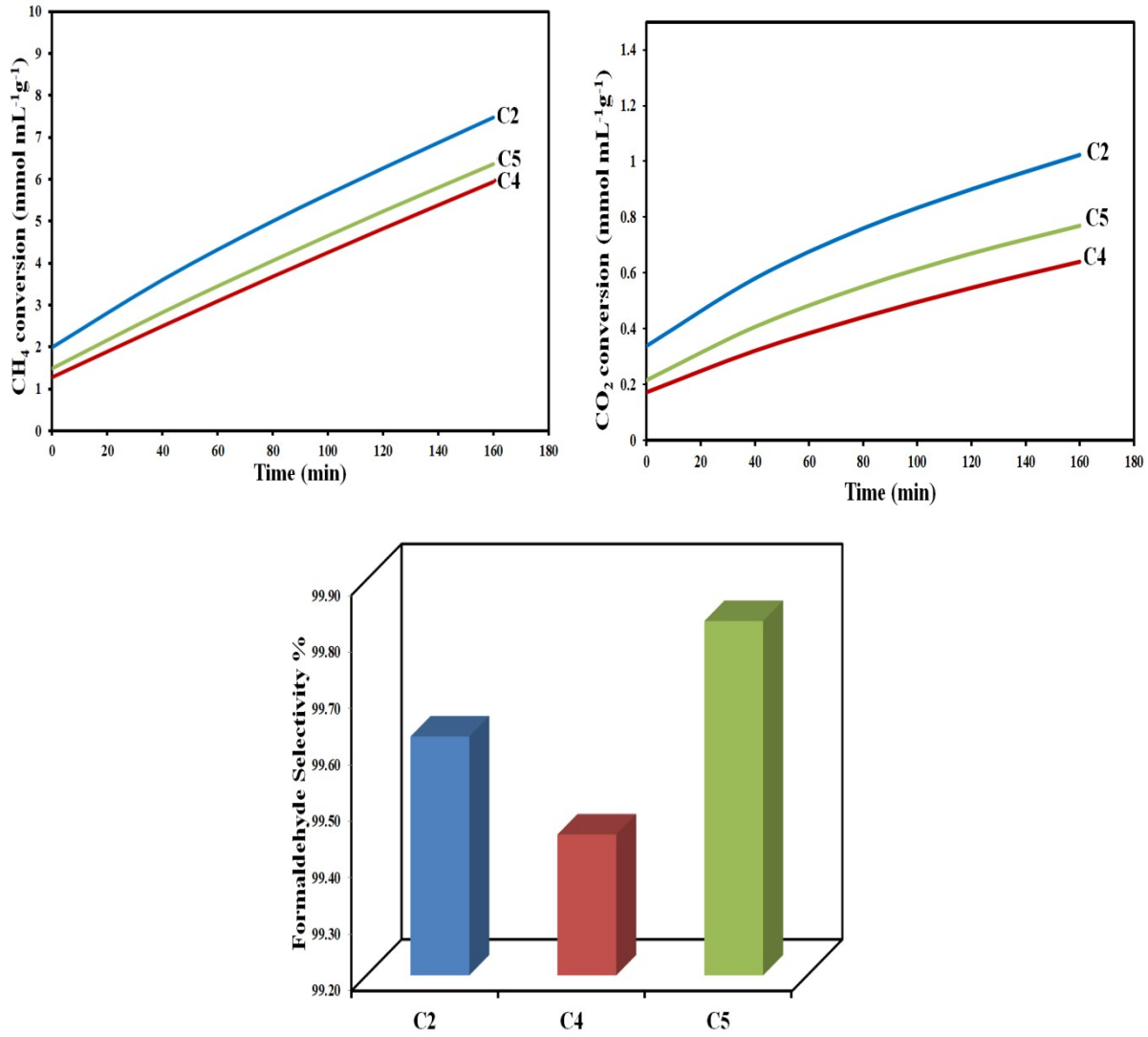

Fig. S17: Accumulative converted amount of CH_4 and CO_2 with time and corresponding formaldehyde selectivity % using the Cu-Al LDH catalysts prepared at different urea concentrations.

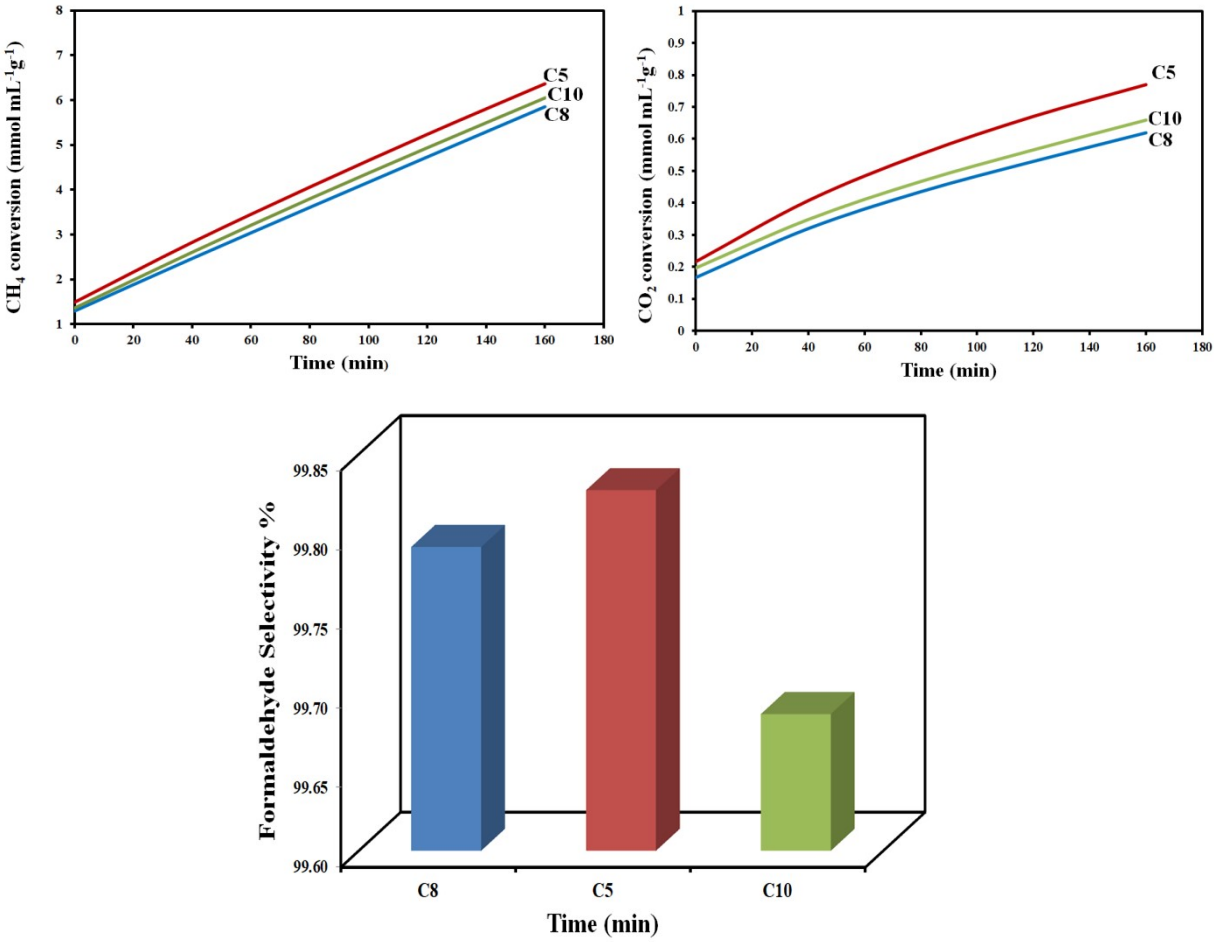

Fig. S18: Accumulative converted amount of CH_4 and CO_2 with time and corresponding formaldehyde selectivity % using the Cu-Al LDH catalysts prepared at different M^{II}/M^{III} ratios.

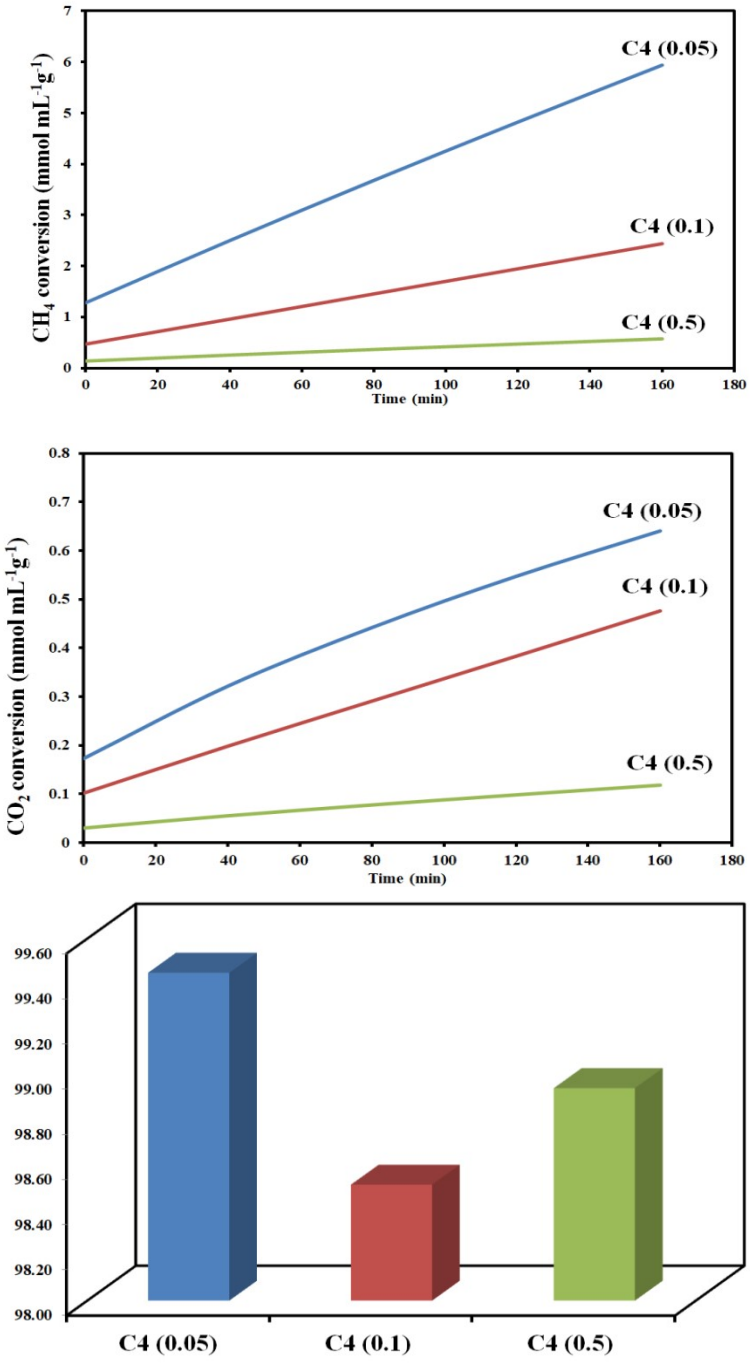

Fig. S19: Accumulative converted amount of CH_4 and CO_2 with time and corresponding formaldehyde selectivity % using different C4 doses.

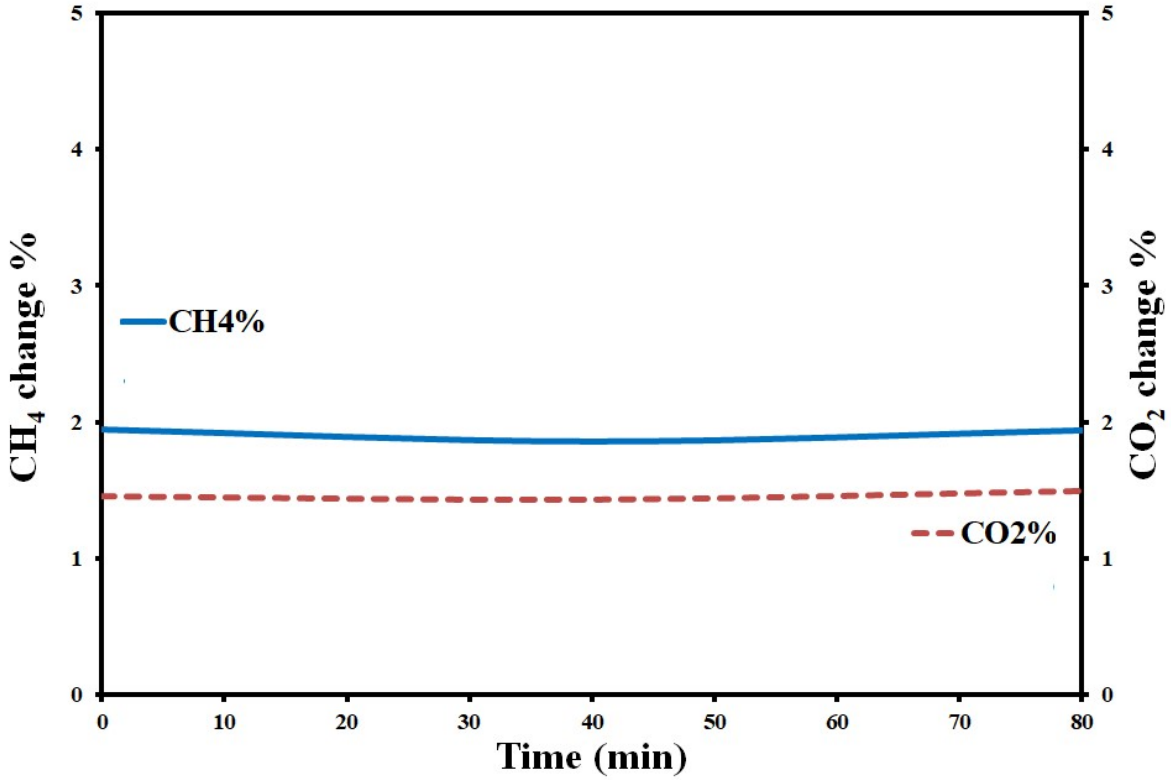

Fig. S20: Variation in both CH_4 and CO_2 percentage with time in light off expermint without catalyst.

References

1 F. Zhao, L. Fan, K. Xu, D. Hua, G. Zhan and S. F. Zhou, *J. CO2 Util.*, 2019, **33**, 222–232.

2 J. Li, S. Zhang, Y. Chen, T. Liu, C. Liu, X. Zhang, M. Yi, Z. Chu and X. Han, *RSC Adv.*, 2017, **7**, 29051–29057.

3 M. Abbasi, M. M. Sabzehmeidani, M. Ghaedi, R. Jannesar and A. Shokrollahi, *Mater. Sci. Eng. B Solid-State Mater. Adv. Technol.*, 2021, **267**, 115086.

4 M. Kiani, M. Bagherzadeh, A. M. Ghadiri, P. Makvandi and N. Rabiee, *Sci. Rep.*, 2022, **12**, 9461.

5 S. P. Adhikari, G. P. Awasthi, K.-S. Kim, C. H. Park and C. S. Kim, *Dalt. Trans.*, 2018, **47**, 4455–4466.

6 M. Ashrafizadeh, E. Nazarzadeh Zare, F. Rossi, N. Rabiee, E. Sharifi and P. Makvandi, *Chem. Eng. J.*, 2022, **448**, 137747.

7 N. Fu, S. Zhang, Y. Ma, Z. Yang and W. Liu, *RSC Adv.*, 2020, **10**, 9808–9813.

8 P. A. Kumar, P. V. Suneesh, B. K. G. Nair and T. G. S. Babu, *Electrochim. Acta*, 2021, **395**, 139145.

9 F. Zhao, G. Zhan and S. F. Zhou, *Nanoscale*, 2020, **12**, 13145–13156.

10 G. Jiang, M. Peng, L. Hu, J. Ouyang, X. Lv, Z. Yang, X. Liang, Y. Liu and H. Liu, *Chem. Eng. J.*, 2022, **435**, 134853.

11 X. Peng, M. Wang, F. Hu, F. Qiu, T. Zhang, H. Dai and Z. Cao, *J. Environ. Manage.*, 2018, **220**, 173–182.

12 P. Benito, M. Herrero, F. M. Labajos and V. Rives, *Appl. Clay Sci.*, 2010, **48**, 218–227.

13 M. Baghbanzadeh, L. Carbone, P. D. Cozzoli and C. O. Kappe, *Angew. Chem. Int. Ed.*, 2011, **50**, 11312–11359.

14 M. V. Sivaiah, S. Petit, J. Brendl?? and P. Patrier, *Appl. Clay Sci.*, 2010, **48**, 138–145.

15 Y. Fernández, J. A. Menéndez, A. Arenillas, E. Fuente, J. H. Peng, Z. B. Zhang, W. Li and Z. Y. Zhang, *Solid State Ionics*, 2009, **180**, 1372–1378.

16 S. C. Zhang and X. G. Li, *Colloids Surfaces A Physicochem. Eng. Asp.*, 2003, **226**, 35–44.

17 C. Feng, Q. Wei, S. Wang, B. Shi and H. Tang, *Colloids Surfaces A Physicochem. Eng. Asp.*, 2007, **303**, 241–248.

18 R. J. M. J. Vogels, J. T. Kloprogge and J. W. Geus, *J. Colloid Interface Sci.*, 2005, **285**, 86–93.

19 A. Naghash, T. H. Etsell and B. Lu, *J. Mater. Chem.*, 2008, **18**, 2562–2568.

20 A. A.-E. Sakr, T. Zaki, O. Saber, S. A. Hassan, A. K. Aboul-Gheit and S. Faramawy, *J. Taiwan Inst. Chem. Eng.*, 2013, **44**, 957–962.

21 S. Nayak and K. M. Parida, *ACS Omega*, 2018, **3**, 7324–7343.

22 K. Parida, L. Mohapatra and N. Baliarsingh, *J. Phys. Chem. C*, 2012, **116**, 22417−22424.

23 G. D. Gesesse, A. Gomis-berenguer, M. Barthe and C. O. Ania, *J. Photochem. Photobiol. A Chem.*, 2020, **398**, 112622.